Journal of Colloid and Interface Science xxx (xxxx) 1–10

Contents lists available at ScienceDirect

Journal of Colloid and Interface Science

journal homepage: www.elsevier.com

Effects of chemical etching and reduction activation on CO oxidation of CeO_2 nanorods supported ruthenium catalysts

Yifan Wang, Ruigang Wang

Department of Metallurgical and Materials Engineering, The University of Alabama, Tuscaloosa, AL 35487, United States

ARTICLE INFO

Article history:
Received 28 October 2021
Received in revised form 9 January 2022
Accepted 9 January 2022

Keywords:
CeO_2 nanorods support
Chemical etching
CO oxidation
In-situ DRIFTS
Ruthenium

ABSTRACT

In this work, pristine and $NaBH_4$ etched CeO_2 nanorods supported ruthenium (Ru) catalysts were synthesized and employed to investigate the effects of chemical etching and reduction activation treatment on CO oxidation. With 1 wt% Ru loading, the CeO_2 nanorods supported catalyst sample, after 6 wt% $NaBH_4$ etching treatment, showed significantly promoted H_2 consumption under 100 °C and low apparent activation energy ($E_a \sim 31.2$ kJ/mol) for CO oxidation. *In-situ* CO-DRIFTS profiles revealed that, for the reduced sample, the observed CO adsorption at ~ 2020 cm^{-1} at 40 °C may be related to a strong RuO_x-CeO_2 interaction induced by the $NaBH_4$ etching process, which were consistent with the oxygen vacancy analysis results of X-ray photoelectron spectroscopy and CO-temperature programmed desorption. The enriched surface defects on CeO_2 support surface due to the chemical etching and reduction treatment are believed to promote the interaction between RuO_x species and CeO_2, which is responsible for the enhanced activity of CO oxidation.

1. Introduction

CO oxidation, as a fundamental reaction in vehicle three-way catalytic converters, is still one of the most important and extensively studied catalytic reactions. Compared to other commonly used platinum group elements, such as palladium (Pd), platinum (Pt) and rhodium (Rh), ruthenium (Ru) has recently attracted significant attention in the fields of noble-metal catalysts with various applications including electrocatalytic CO_2 reduction and reuse, water splitting, and CO/hydrocarbon catalytic oxidation due to its comparably lower cost and excellent activity. Especially for CO oxidation, Ru-based catalysts exhibit enormous potential with outstanding activity at low temperatures. For example, Huang et al. [1] reported on novel solid-solution alloy nanoparticles of Ru and Cu, demonstrating higher CO oxidation activity than fcc Ru which is one of the best monometallic CO oxidation catalysts. Wang et al. [2] constructed a Ru-Co_3O_4 interface, which can activate the O_2 species at the interface, resulting in lowered activation energy and boosted catalytic performance of CO oxidation. Kim et al. [3] prepared Ru catalysts supported on various aluminum oxides with different crystalline phases and found Ru/α-Al_2O_3 can reduce a high inlet concentration of CO to less than 10 ppm even in the presence of H_2O and CO_2 over a wide temperature range.

Ceria (CeO_2) is well-known for its excellent oxygen storage capacity and high redox ability via a reversible Ce^{4+} to Ce^{3+} transition [4,5]. CeO_2 can act as an active component in many redox-related catalytic reactions and has been extensively studied. CeO_2 nanocrystals with different morphologies, such as nanoctahedra, nanospheres, nanocubes, and nanorods (NR) have been studied to understand the effects of nanoparticle morphology and exposed crystal planes on the activity and selectivity of CeO_2 supported metal or metal oxide catalysts [6–8]. According to others' and our previous work [9–11], CeO_2 nanorods (CeO_2NR) supported metals or metal oxides (i.e. Ru and CuO_x) show superior activity in water–gas shift reaction and CO oxidation compared to CeO_2 nanocubes (CeO_2NC) and nanoctahedra (CeO_2NO) supported metals or metal oxides, thanks to the exposed crystal planes and surface defects.

In addition to utilization of catalytically active supports, surface modification of supports and catalysts has also been widely adopted to further enhance the performance of existed catalysts system for economic and large-scale practical applications [12,13]. For instance, Gao et al [14] reported that surface engineering of CeO_2NR by chemical redox etching resulted in rough, high porosity catalyst surfaces, which can increase the catalytic activity for CO oxidation due to the enhancement of specific surface area, oxygen vacancy content and the surface Ce^{3+} fraction of CeO_2NR. Han et al. [15] reported the effect of sulfate acid pretreatment on CeO_2/ZrO_2 catalysts to promote the selective catalytic reduction. Furthermore, Baechong et al [16] studied the catalytic activity of nanoscale zero-valent iron (Fe^0) after $NaBH_4$ etching for reduction of p-nitrophenol and found that the addition of $NaBH_4$ initiated the disintegration of iron species into smaller clusters with increased reactive surface.

Based on the literature and above findings, chemical etching (or surface modification) can directly modify the surface of CeO_2NR support

https://doi.org/10.1016/j.jcis.2022.01.062
0021-9797/

and show significant influence on the catalytic activity of supported transition metal catalysts. However, the exact effects of chemical etching to CeO_2 supported catalysts need to be revealed to further comprehensively understand the role of surface chemistry in the interaction between Ru species and CeO_2NR support. In this study, CeO_2NR was first chemically etched by strong reducing agent $NaBH_4$ (hereinafter referred to as mCeO_2NR; "m" refers to "modified") and then mCeO_2NR supported 1 wt% ruthenium oxide catalysts were prepared and used to study the effect of chemical etching on the surface chemistry and resulting CO oxidation. Temperature and time dependent in-situ diffuse reflectance infrared Fourier transform spectroscopy (DRIFTS) was used to elucidate the mechanisms of CO adsorption, which can be further used to investigate the catalysts behavior during CO oxidation. The effect of strong interactions between Ru species and mCeO_2NR on CO oxidation is discussed.

2. Experiment

2.1. Preparation of pristine CeO_2NR support

A hydrothermal method was used to synthesize CeO_2NR support. According to our previous study [17,18], 8.8 mmol cerium nitrate hexahydrate ($Ce(NO_3)_3{\cdot}6H_2O$, Sigma Aldrich, 99%) was dissolved in 88 mL deionized water (DI water). Then, 8 mL of aqueous solution containing 48 mmol NaOH was added dropwise with a pipette into the $Ce(NO_3)_3$ solution with simultaneous mild stirring until the formation of a milky slurry. After that, the mixture was transferred into a Teflon lined stainless-steel autoclave and aged at 90 °C for 48 h. To obtain dry, pristine CeO_2NR powder, the sample was filtered and dried at 60 °C overnight.

2.2. $NaBH_4$ chemical etching treatment of CeO_2NR powder

To obtain surface modified CeO_2NR (m-CeO_2NR) support, strong reducing agent $NaBH_4$ was used to etch and tune the surface structure/chemistry of the pristine CeO_2NR powder in the following steps [19]. 0.5 g CeO_2NR powder was dispersed in 250 mL of DI water with vigorous stirring, and 6 wt% $NaBH_4$ (powder, ≥98.0% from Sigma-Aldrich) was added to the CeO_2NR suspension. After stirring at room temperature for 12 h, the mixture suspension was then filtered and dried at 60 °C overnight. Then the powder sample was finally calcined at 300 °C for 5 h in air.

2.3. Deposition of ruthenium oxide catalysts on CeO_2NR

CeO_2NR/mCeO_2NR supported RuO_x catalysts were prepared by co-precipitation method. First, 0.5 g of CeO_2NR or mCeO_2NR was added to 100 mL DI water with mild stirring on a magnetic stirrer. Then the required amount of Ru precursor ($Ru(NO)(NO_3)_3$, Alfa Aesar) was added to the CeO_2 suspension to obtain 1 wt% of Ru loading. Aqueous ammonia ($NH_3{\cdot}H_2O$) was added dropwise into the $Ru(NO)(NO_3)_3$/CeO_2NR or $Ru(NO)(NO_3)_3$/mCeO_2NR suspension until a pH value of 7 was reached. The resulting solution was heated to 80 °C for 4 h on a hot plate, and then the temperature was increased to 100 °C until a complete water evaporation. The dried catalyst powders were calcined at 300 °C for 5 h under air flow with a heating ramp of 10 °C /min to obtain homogeneous supported RuO_x catalysts. The calcined samples were denoted as RuO_x-CeO_2NR-o or RuO_x-mCeO_2NR-o (1 wt% = $[Ru/(Ru + CeO_2)]_{wt} \times 100\%$). The reduced supported RuO_x catalysts were synthesized by reducing part of the oxidized Ru catalysts at 300 °C°C for 5 h with a heating ramp of 10 °C /min in a 5.0 vol% H_2/Ar flow (200 mL/min). Finally, RuO_x-CeO_2NR-r or RuO_x-mCeO_2NR-r catalysts were obtained after the furnace was cooled down to room temperature with the same 5.0 vol% H_2/Ar flow.

2.4. Catalyst characterizations

The crystalline structure of supported RuO_x catalysts was analyzed by X-ray diffraction on a Philips X'Pert MPD diffractometer with Cu Kα radiation source (λ = 1.5418 Å). The XRD profiles were recorded in a range of 2θ from 5° to 90° with scanning rate of 0.01° per second. The working voltage and current for the X-ray diffractometer were 45 kV and 40 mA, respectively. The Ru content of supported RuO_x catalysts were determined using Apreo scanning electron microscope with an energy-dispersive X-ray spectroscopy (Bruker XFlash EDS) detector at the accelerating voltage of 20 kV. The samples of EDS were prepared by placing small amount of powder on conductive carbon tapes with a flat surface.

Horiba Labram HR 800 Raman Spectrometer was used for the Raman spectra of catalysts, using 532 nm laser module scanned in the range of 100–1500 cm^{-1}. A FEI Tecnai F20 operated at 200 kV, equipped with a high angle annular dark field detector (HAADF) and an EDAX detector, was used for transmission electron microscopy (TEM) and scanning transmission electron microscopy (STEM) with EDS analysis. The samples were prepared by dispersing powder in ethanol with ultrasonic and then dropping onto an ultrathin holey carbon film supported on copper grid (from Ted Pella). A Kratos Axis Ultra DLD spectrometer with monochromatic Al K_α radiation ($h\nu$ = 1486.6 eV) was used under ultra-high vacuum (UHV) conditions with base pressure under 8×10^{-10} Torr for X-ray photoelectron spectroscopy (XPS) data acquisition and CASAXPS software for data analysis. After mixing catalyst powders into ethanol with ultrasonic, the 2–3 droplets of suspension were then transferred on flat silicon wafer. The final thin-film sample were obtained after ethanol evaporation in air. The carbonaceous C 1s line at 284.8 eV was used to calibrate the binding energies as an internal standard.

The specific surface areas of the powder samples were obtained according to the Brunauer-Emmett-Teller method (BET) by measuring N_2 adsorption/desorption at ~ -196 °C through the signal from a thermal conductivity detector (TCD) on the Micromeritics AutoChem II 2920 chemisorption analyzer. Hydrogen temperature programmed reduction (H_2-TPR), carbon monoxide temperature programmed desorption (CO-TPD) and oxygen temperature programmed desorption (O_2-TPD) were carried out on the same chemisorption analyzer to acquire information on the reducibility and CO adsorption/desorption ability of the samples, respectively. For a typical H_2-TPR experiment, powder sample (~90 mg) was placed in a quartz U-tube reactor and heated up from 30 °C to 900 °C at a heating rate of 10 °C /min with 10% H_2 /Ar gas flow (flow rate: 50 mL/min). For CO-TPD/O_2-TPD, 50 mg of catalyst was first pretreated with He gas flow (flow rate 50 mL/min) at 400 °C for 1 h to remove residual surface moisture. Second, the catalyst was saturated by 10% CO/He gas flow for CO-TPD or 5% O_2/He has flow for O_2-TPD (flow rate 50 mL/min) at 30 °C for 1 h, and then flushed with He gas flow (flow rate 50 mL/min) from 30 °C to 900 °C to monitor the desorption behavior.

A Bruker Vertex 70 FTIR spectrometer equipped with a Harrick cell and a room temperature DLaTGS detector was used for *In-situ* diffuse reflectance infrared spectroscopy (DRIFTS). The catalyst powders were flushed by UHP N_2 gas inside the cell with a flow rate of 30 mL/min at 200 °C for 30 min to remove residual surface moisture. After temperature back to 35 °C, the background spectrum was collected at the same flow of N_2. The temperature-dependent *in-situ* DRIFTS spectra were collected with 30 mL/min 5 vol% CO/95 vol% Ar mixture feeding gas with the temperature ramping from 35 °C to 150 °C with a heating rate of 10 °C/min. The interval of each spectrum for temperature dependences is 10 °C and the first one started at 40 °C. For the time-dependent *in-situ* DRIFTS spectra, the catalysts went through the same pre-treatment as the temperature-dependent experiments. After the collection of background spectrum, the feed gas switched to a 30 mL/min 5 vol% CO/95 vol% Ar mixture feeding gas for 40 min, after which the

flow was switched back to 30 mL/min UHP N_2 gas for 40 min. During the whole time, the DRIFTS spectra were continuously recorded every 10 min by collecting 64 scans with a resolution of 4 cm^{-1}.

2.5. Catalytic activity measurements

The CO oxidation activity toward CO conversion were carried out with a fixed bed plug flow reactor system, loaded 50 mg of catalyst with quartz wool. The total flow rate of the feed gas (1 vol% CO/20 vol% O_2/He gas flow) was 30 mL/min, corresponding to a weight hour space velocity (WHSV) of 36,000 mL h^{-1} g_{cat}^{-1}. The measurements were carried out by heating the reactor from room temperature to 400 °C. The reactants and products were analyzed by an online gas chromatograph (SRI multiple gas analyzer GC, 8610C chassis) system. The catalytic stability test for CO conversion was carried out with the same system of the activity test. The sample was heated to the experimental temperature that provides ~ 90% CO conversion and was kept at that temperature for 24 h. The effect of water vapor was studied with RuO_x-$mCeO_2$NR-r. The water vapor was carried by N_2 through a water bubbler at room temperature. The conversion of CO (C_{CO}) was defined according to the following equation:

$$C_{co}(\%) = ([CO]_{in} - [CO]_{out})/[CO]_{in} \times 100$$

Where $[CO]_{in}$ is the influent CO concentration and $[CO]_{out}$ is the effluent CO concentration.

3. Results and discussion

3.1. Morphological and structural characterizations

The XRD patterns of Ru catalysts supported by unmodified/modified CeO_2NR before and after reduction treatment at 300 °C in 5.0 vol% H_2/Ar are shown in Fig. 1. Among the four samples, there is no observable phases for Ru species, owing to the low content of Ru (1 wt%) and/or the excellent dispersion/diffusion of Ru species into CeO_2NR lattice. It has been reported previously that the surface defects of CeO_2NR support promote the ionic diffusion interaction between catalyst and support [9]. All observed diffraction peaks at 28.5, 33.1, 47.5, 56.3, 59.1 69.4, 76.7, 79.1 and 88.4° correspond to the face-centered cubic CeO_2 phase with fluorite structure (JCPDS #34–0394). For the unmodified/

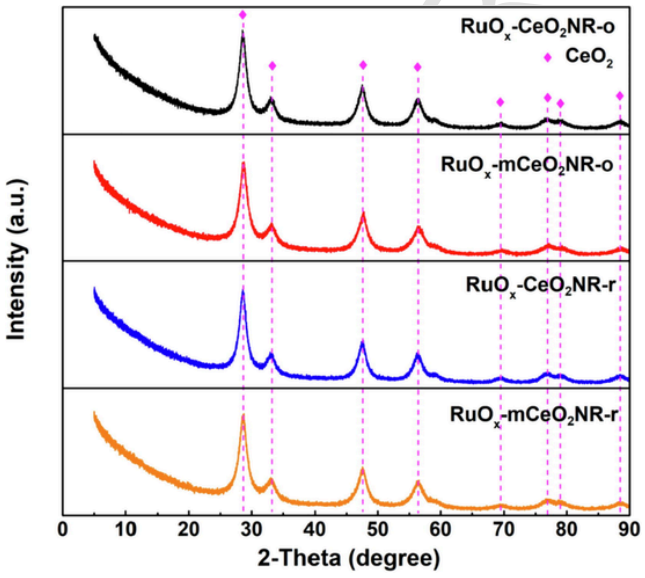

Fig. 1. XRD patterns of unmodified/modified CeO_2NR supported Ru catalysts before and after the reduction treatment.

modified CeO_2NR supports without Ru loading, they showed very similar XRD patterns according to our previous work [20].

It can be clearly observed from the Raman spectra in **Fig. S1** that the integrated area of D band follows the order of RuO_x-$mCeO_2$NR-r > RuO_x-CeO_2NR-r > RuO_x-$mCeO_2$NR-o > RuO_x-CeO_2NR-o, which is consistent with the results of oxygen vacancy obtained from the XPS spectra of O 1 s region. Moreover, RuO_x-$mCeO_2$NR-r shows a redshift of peak for 2TA mode vibration, indicating the lower symmetry of Ce-O bond or lattice distortion due to the possible formation of the Ru-O-Ce bonds.

The TEM and HRTEM images of four Ru/CeO_2NR catalysts are shown in Fig. 2. It can be observed that the unmodified CeO_2NR support has a length of 50–80 nm and diameter of 5–10 nm after the Ru loading and thermal treatments. And the modified CeO_2NR after the oxidation treatment has a length of 30–70 and diameter of 3–7 nm, which is a little shorter and thinner than unmodified CeO_2NR. There is no significantly visible change of particle size or shape after the reduction treatment. The HRTEM images of individual support particles exhibit a lattice fringes spacing with 0.31 nm that can be assigned to (1 1 1) surface termination of CeO_2, and the lattice spacing of 0.27 nm is associated with the (2 0 0) surface of CeO_2. In these supported catalyst particles the apparent absence of large Ru clusters or nanoparticles suggests good Ru dispersion on the CeO_2NR and/or possible Ru-O-Ce alloying, which is consistent with the XRD analysis. In addition, Fig. S2-S5 show the STEM images and EDS elemental mapping for RuO_x-CeO_2NR-o, RuO_x-$mCeO_2$NR-o, RuO_x-CeO_2NR-r and RuO_x-$mCeO_2$NR-r, respectively. The EDS mapping results in Fig. S2-S4 exhibit the good dispersion of Ru species on CeO_2NR supports.

3.2. Catalytic properties and XPS analysis

The H_2-TPR profiles of pristine and $NaBH_4$ modified CeO_2NR supported Ru catalysts, after oxidation or reduction treatment, are presented in Fig. 3**(a)**. Owing to the strong H_2 consumption at low temperature region (below 250 °C) [9,20], the hydrogen consumption peak at higher temperature region was attributed to the surface and bulk reduction of CeO_2NR and $mCeO_2$NR supports, which was relatively small when compared to low temperature reduction, suggesting a dominant low temperature RuO_x-related reduction. For the low temperature region, RuO_x-CeO_2NR-o sample showed three reduction peaks at 100, 117 and 130 °C, while RuO_x-$mCeO_2$NR-o sample presented two reduction peaks at 110 and 125 °C. The presence of multiple reduction peaks for oxidized Ru catalysts indicates different coordination environments of Ru or different valence states of Ru species on the surface of CeO_2NR [21]. The peak appeared at 100 °C for RuO_x-CeO_2NR-o was ascribed to the well-dispersed smaller size RuO_x species that can be reduced at much lower temperature when compared to the well crystallized or agglomerated RuO_2 [9], which explains the existence of peaks at 125 and 130 °C. Compared to the reduction peak at 100 °C, the extra peak at 117 °C for RuO_x-CeO_2NR-o might be owing to the well-dispersed RuO_x on CeO_2NR surface [22]. The peak at 110 °C of the $mCeO_2$NR supported Ru catalyst can be assigned to the chemisorbed oxygen (O^- or O_x^-) promoted RuO_x reduction, which is similar to Wu et al's report that Ag catalysts supported by CeO_2 with different surface oxygen species were reduced at different temperature [23]. For the reduced samples, one main peak at 94 °C and a shoulder peak at 102 °C were showed for the RuO_x-CeO_2NR-r sample. And the RuO_x-$mCeO_2$NR-r sample showed similar profiles with one main peak at 94 °C and a shoulder peak at 82 °C. The main reduction peak can be ascribed to the reduction of RuO_x with strong RuO_x-CeO_2 interaction, which is because the Ru species activate oxygen ions on CeO_2NR surface and can be easily transferred and employed [24]. The different reduction temperature of two shoulders may be owing to different chemically coordinated states of Ru species. According to our previous study [19,20], $NaBH_4$ modified CeO_2NR presented more surface defects and these defects acted as active sites for

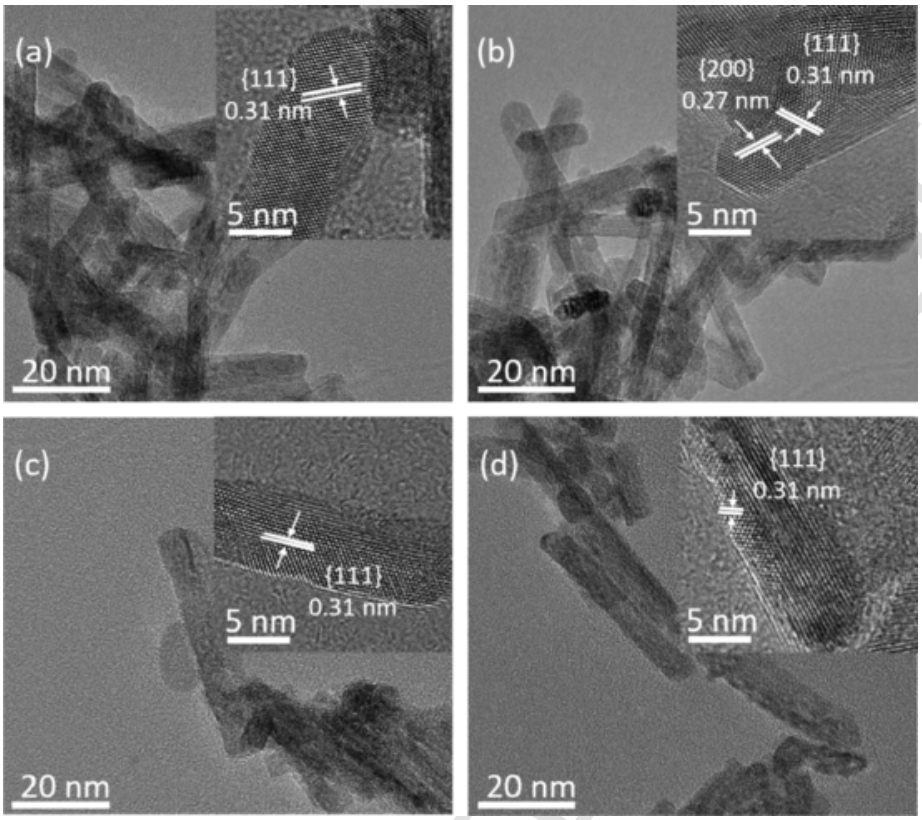

Fig. 2. TEM and HRTEM images of (a) RuO_x-CeO_2NR-o, (b) RuO_x-mCeO_2NR-o, (c) RuO_x-mCeO_2NR-o and (d) RuO_x-mCeO_2NR-r.

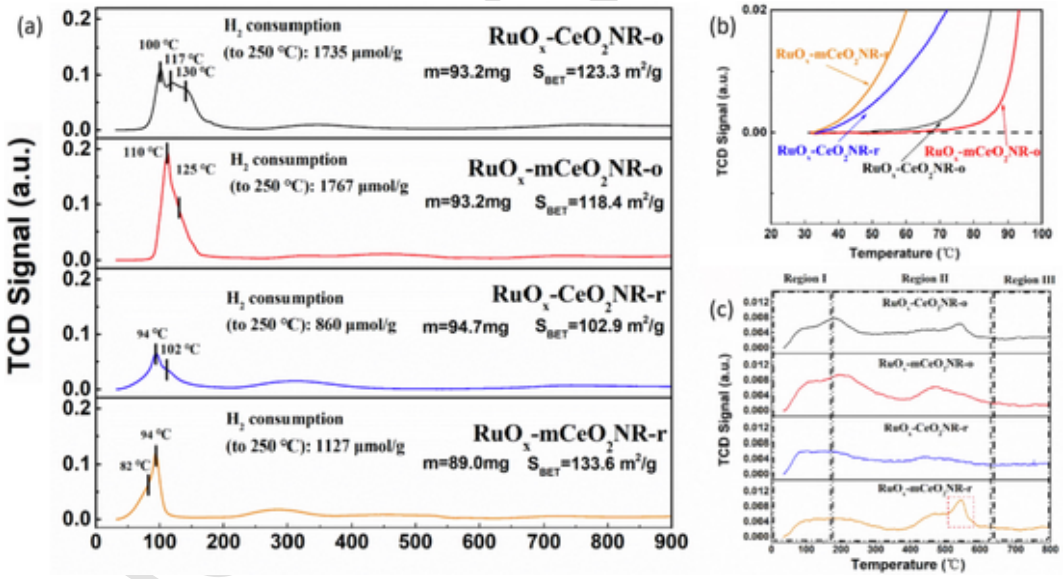

Fig. 3. (a) H_2-TPR profiles of unmodified/modified CeO_2NR supported Ru catalysts before and after the reduction treatment and (b) low temperature TPR region showing the initial reduction between 20 and 100 °C. (c) CO-TPD profiles.

catalyst clusters trapping and anchoring. Therefore, the Ru species with defect rich m-CeO_2NR surface showed stronger RuO_x-CeO_2 interaction that can be reduced at lower temperature. On the other hand, the higher H_2 consumption of RuO_x-mCeO_2NR-r also supports the enhancement effect of chemical etching modification on low temperature reduction as shown in Table 1. The BET surface area of the RuO_2-CeO_2NR-o (123.3 m^2/g) and RuO_x-mCeO_2NR-o (118.4 m^2/g) sample are similar. However, the BET surface area of the unmodified CeO_2NR supported Ru catalysts decreased after reduction treatment, which might be attributed to the sintering of Ru species during the high temperature reduction treatment.

Fig. 3**(b)** showed the on-set reduction temperature of four supported Ru catalysts. It can be observed that: the reduced Ru catalysts presented much lower "onset" reductivity when compared to the oxidized catalysts, indicating that the reduction treatment may promote a strong RuO_x-CeO_2 interaction. As a result of $NaBH_4$ modification, RuO_x-mCeO_2NR-r apparently showed the lowest reduction onset temperature, which agrees with the result of H_2 consumption summarized in Table 1. On the other hand, compared with the unmodified CeO_2NR

Table 1
Ru content, BET surface area, H_2 consumption and initial reduction temperature of Ru catalysts supported by CeO_2NR.

Sample	Ru content (wt.%)	BET surface area m^2/g	H_2 consumption (30 °C to 250 °C) μmol/g	Onset reduction temperature °C	Initial H_2 consumption rate (30 °C to 90 °C) μmol/(g*s)
RuO_x-CeO_2NR-o	0.94	123.3	1735	78	0.36
RuO_x-mCeO$_2$NR-o	0.78	118.4	1767	91	0.03
RuO_x-CeO_2NR-r	0.89	102.9	860	57	0.66
RuO_x-mCeO$_2$NR-r	0.75	133.6	1127	50	1.36

supported Ru catalysts, RuO_x-mCeO$_2$NR-o and RuO_x-mCeO$_2$NR-r showed an extra reduction peak and lower reduction temperature between 200 °C and 900 °C (**Fig. S6**), indicating the promotion effect of $NaBH_4$ etching on the reducibility of the CeO_2NR supports and supported catalysts.

The CO-TPD profiles of the CeO_2NR supported Ru catalysts are illustrated in Fig. 3**(c)**. The CO desorption profiles of the supported catalysts can be divided into three different peak regions [25–27]. The peak region I from room temperature to 180 °C is assigned to the CO_2 desorption from CO oxidation with overactive surface oxygen species, and the peak region II from 180 °C to 650 °C can be assigned to the CO_2 desorption from CO oxidation through lattice oxygen species of CeO_2 and the conversion of surface and interface carbonates. The peak region III from 650 °C to 800 °C corresponds to the CO_2 desorption from decomposition of carbonate species. It should be noted that the strong peak for RuO_x-mCeO$_2$NR-r near 550 °C indicates a different type of CO_2 desorption site, which could be due to the different oxygen species on the modified CeO_2NR surface. Additionally, according to the O_2-TPD patterns from **Fig. S7**, all the Ru catalysts show the better oxygen adsorption than CeO_2NR supports with/without modification. Moreover, RuO_x-mCeO$_2$NR-r shows the highest total amount of chemically adsorbed oxygen species, which is consistent with the results obtained from Raman and XPS.

By analyzing the Ce 3d spectra, the chemical states and concentration of cerium ions (Ce^{3+}/Ce^{4+}) on the surface of different CeO_2NR supports were investigated and shown in Fig. 4**(a)**. The calculated concentrations of cerium, ruthenium and oxygen species are summarized in Table 2. Corresponding to the $3d_{3/2}$ and $3d_{5/2}$ spin–orbit coupling, the spectra of Ce 3d can typically be divided into 10 peaks, where the peaks v_0, v', u_0 and u' ascribe to the Ce^{3+} state, while the peaks v, v", v"', u, u", u"' attribute to the Ce^{4+} state[28]. The concentration fraction of Ce^{3+} to the total Ce species was calculated by the integrated peak areas of Ce^{3+} and Ce^{4+} from the Ce 3d spectra [29]. As shown in Fig. 4**a**, the concentration fraction of Ce^{3+} is 9.0% for RuO_x-CeO_2NR-o, 9.3% for RuO_x-mCeO$_2$NR-o, 10.4% for RuO_x-CeO_2NR-r and 10.8% for RuO_x-mCeO$_2$NR-r. It is known that Ce^{3+} ions prefer to form with the vicinity of oxygen vacancy and other types of surface defects [30]. On the other hand, Ce^{3+} can also present near the doping sites of Ru ions to balance the charge difference (Ru^{4+}, Ru^{6+} and Ce^{4+}).Table 3

The O 1s spectra for the CeO_2NR supported Ru catalysts are displayed in Fig. 4**(b)**. In literature, the observed O 1s peaks around 530 eV in CeO_{2-x} ($0 \le x \le 0.5$) are typically ascribed to three kinds of oxygen species: lattice oxygen (O_L); vacancy related oxygen species (O_V); and surface-chemisorbed oxygen species (O_C) or oxygen in hydroxyl groups (O_{OH}) [11,31]. Due to the high surface concentration of oxygen vacancy in the prepared CeO_2NR [14–17,24], the peaks at 529.4, 531.5 eV, 532.3 eV and 533.8 eV are assigned to lattice oxygen (O_L), oxygen vacancy/defects (O_V), surface-chemisorbed oxygen species (O_C) or oxygen in hydroxyl groups (O_{OH}) on the surface of CeO_2NR, respectively. Pu et al [32] studied the Pr- and Cu- doped CeO_2 catalysts, proposing a possible pathway for CO oxidation, where the first step was believed to involve the O_2 chemisorption on the catalyst surface and highly associate with sites like the oxygen vacancy (O_v). As shown in Fig. 4**(b)**, the relative concentration of O_v is calculated by the

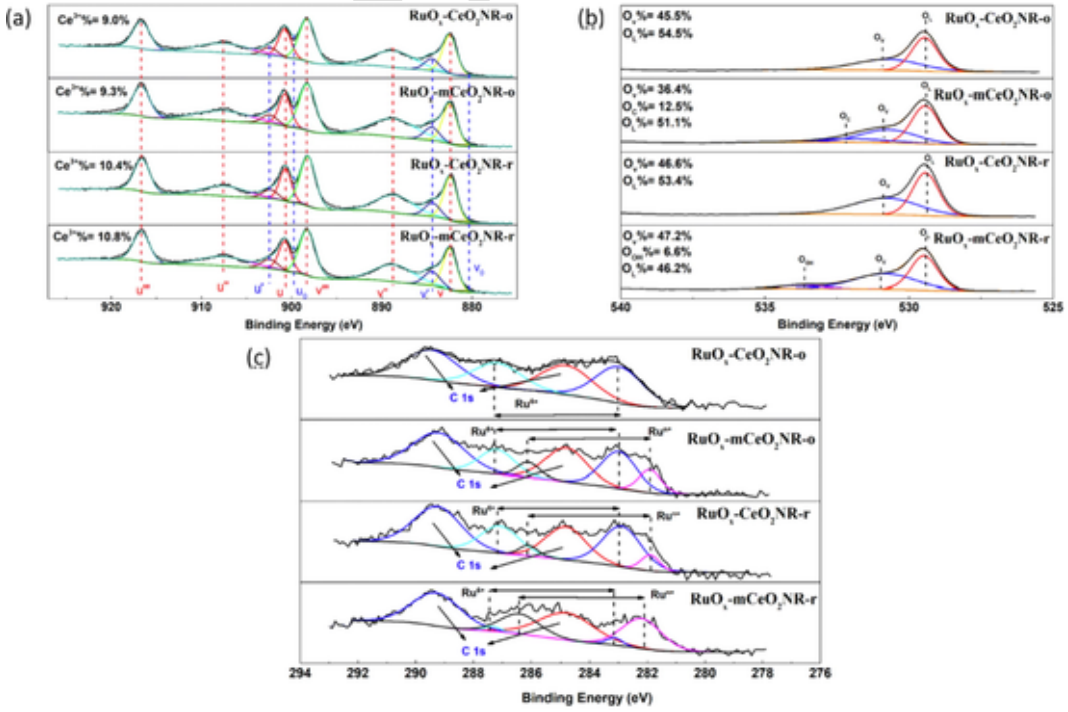

Fig. 4. XPS spectra of (a) Ce 3d, (b) O 1s, and (c) Ru 3d for unmodified/modified CeO_2NR supported Ru catalysts before and after the reduction treatment.

Table 2
Concentration of Ce^{3+}, Ru^{6+}/Ru^{n+} and O_v of Ru catalysts.

Sample	Ce^{3+} (at.%)	Ru^{6+} (at.%)	Ru^{n+} (at.%)	Ov/O_{total} (at.%)
RuO_x-CeO_2NR-o	9.0	100	0	45.5
RuO_x-mCeO_2NR-o	9.3	71.7	28.3	36.4
RuO_x-CeO_2NR-r	10.4	82.2	17.8	46.6
RuO_x-mCeO_2NR-r	10.8	8.6	91.7	47.2

Table 3
Peak assignments of *in situ* DRIFTS spectra for CeO_2NR supported Ru catalysts.

Wavenumber (cm^{-1})	Description	Ref
~2180	CO gas	[39]
~2130/ ~2060	CO– $Ru^{\delta+}$	[39, 40]
~2044	CO-Ru^0	[41, 42]
~2020	CO-Ru^0	[43]
~1999	CO adsorbed on oxygen vacancies or the CO IR-adsorption band which is unique to Ru-doped CeO_2	[39, 44]
~1977	CO-Ru at Ru-CeO_2 interface	[45]
~1873/ ~1844	CO-O_v at Ru-CeO_2 interface	[43]

integrated peak area of the oxygen species. The values of the concentration are 45.5%, 36.4%, 46.6% and 47.2% for RuO_x-CeO_2NR-o, RuO_x-mCeO_2NR-o, RuO_x-CeO_2NR-r and RuO_x-mCeO_2NR-r, respectively. In addition, the presence of O_C in RuO_x-mCeO_2NR-o, which is consistent with the H_2-TPR results, indicates that more surface defects and chemisorbed oxygen species were generated by a combination of the $NaBH_4$ etching and RuO_x deposition on the defect rich CeO_2NR surface. These results clearly show the $NaBH_4$ etching effect on chemical and structural changes on the support surface, particularly leading to active surface oxygen species which may be related to their catalytic performance.

Fig. 4**(c)** shows the XPS spectra of Ru 3d for RuO_x-CeO_2NR-o, RuO_x-mCeO_2NR-o, RuO_x-CeO_2NR-r and RuO_x-mCeO_2NR-r. With a little tricky analysis of the Ru $3d_{5/2}$ peaks, the peak at around 282.9 eV can be assigned to the Ru^{6+} for RuO_x-CeO_2NR-o, RuO_x-mCeO_2NR-o and RuO_x-CeO_2NR-r. The peaks at around 281.9 eV are associated with the Ru^{n+} ($4 \le n \le 6$) for RuO_x-mCeO_2NR-o and RuO_x-CeO_2NR-r. It can be observed that the peaks for Ru^{6+} and Ru^{n+} for RuO_x-mCeO_2NR-r shifted to higher binding energy when compared to other Ru catalysts. According to Guo et al's study [33], the charge density of Ru deposits is highly affected by the interfacial charge transfer, indicating that their oxidation states are extremely correlated with the strength of electronic interaction between RuO_x and CeO_2. They found that the Ru catalysts with stronger electronic interaction show slightly higher average valence state of Ru species, exhibiting higher binding energy. Therefore, the higher binding energy of Ru^{n+} and larger amount of Ru^{n+} species imply the stronger RuO_x-CeO_2 interaction for RuO_x-mCeO_2NR-r, which is promoted by the surface defects on modified CeO_2NR surface. The other two intense peaks at around 284.8 eV and 289.2 eV are for C 1s peaks. For the oxidized Ru catalysts, it can be observed that the concentration of Ru^{n+} species increased on mCeO_2NR surface when compared to that of RuO_x-CeO_2NR-o. This can be explained by that Ru^{n+} are most likely formed from the small RuO_x ($0 \le x \le 1$) clusters with the strong RuO_x-CeO_2 interaction at the interface. Compared to the unmodified CeO_2NR supports, the CeO_2NR supports after $NaBH_4$ modification generated large amount of surface defects including oxygen vacancies, steps and voids, which can help anchor and trap Ru ion species and strengthen the interaction between RuO_x and CeO_2 [34]. For the reduced Ru catalysts, the concentration of Ru^{n+} species further increased to 91.7% for RuO_x-mCeO_2NR-r, which is owing to the combination of surface etching effect and reduction treatment induced defects. Both Bhaskar et al [35] and Qadir et al [36] reported that the reduction treatment boosted the formation of Ru^{n+}, which is consistent with the results in this study. Clearly the results of XPS spectra for O 1s region show that RuO_x-mCeO_2NR-r possesses the highest concentration of oxygen vacancy (O_v).

3.3. *In-situ DRIFTS study*

The temperature dependent *in-situ* DRIFTS spectra of CO adsorption on RuO_x-CeO_2NR-o, RuO_x-mCeO_2NR-o, RuO_x-CeO_2NR-r and RuO_x-mCeO_2NR-r are shown in Fig. 5**(a ~ d)**. The initial state (40 °C) and final state (150 °C) of the *in-situ* DRIFTS spectra for four samples are summarized and compared in Fig. 5**(e, f)**. Except for the gas-phase CO signals at around 2180 cm^{-1}, the high-frequency peak at around 2130 cm^{-1}/2060 cm^{-1} for CO adsorption spectra can be assigned to the multicarbonyl species formed by binding two or three CO ligands to $Ru^{\delta+}$ sites [37,38]. The weak band at around 2044 cm^{-1} for RuO_x-CeO_2NR-o can be assigned to the C—O vibrations of linearly adsorbed CO on Ru^0 sites [39,40]. The very weak band at around 2020 cm^{-1} for RuO_x-CeO_2NR-r and RuO_x-mCeO_2NR-r are associated to another linearly adsorbed CO on high defect concentration sites and/or isolated Ru^0 species surrounded by partially oxidized Ru, [CO-Ru^0] [40]. The strong band at around 1990 cm^{-1} for RuO_x-CeO_2NR-o and RuO_x-mCeO_2NR-o is attributed to CO adsorbed on oxygen vacancies or the CO IR-adsorption band which is unique to Ru-doped CeO_2 [37,41]. The similar band at around 1977 cm^{-1} for RuO_x-CeO_2NR-r and RuO_x-mCeO_2NR-r is ascribed to the bridged CO bonded to Ru at Ru-CeO_2 interface [42]. The unique band at 1844 cm^{-1} for RuOx-mCeO_2NR-r can be assigned to the bridged CO bonded with Ru-CeO_2 interface [Ru_2-(CO)] [40].

For RuO_x-CeO_2NR-o, all bonds including CO-$Ru^{\delta+}$, CO-Ru^0 and CO-O_v became stronger with increasing temperature, indicating strong thermal stability at higher temperature (up to 150 °C). For RuO_x-mCeO_2NR-o, all CO adsorption bands are similar to those of RuO_x-CeO_2NR-o, except for the CO-Ru^0 bond. There is no significant signal for CO-Ru^0 in RuO_x-mCeO_2NR-o, indicating the absence of Ru^0 state on surface. Kim et al [43] synthesized Pt/TiO_2 catalysts with different Pt valence state and chemisorbed oxygen species. Their DRIFTS analysis showed that the chemisorbed oxygen species were involved in the formation of formate species, which would react with moisture and form CO-Pt^0 bonds. Therefore, the absence of CO-Ru^0 in RuO_x-mCeO_2NR-o may be due to the inhabitation effect of chemisorbed oxygen species on surface, which would form formate with CO flow rather than direct linear adsorption. This result is consistent with the H_2-TPR and XPS results.

For RuO_x-CeO_2NR-r, the similar bands shifted to lower wavenumber when compared to those of RuO_x-CeO_2NR-o, indicating the lower average valence state of Ru [44]. And there are strong signals for CO gas at around 2180 cm^{-1}, which is even more obvious in Fig. 5**(e)**. The existence of CO gas in spectra reveals the weaker CO absorption capacity of the reduced Ru catalysts than that of the oxidized Ru catalysts. On the other hand, RuO_x-CeO_2NR-r displays no signal at around 2044 cm^{-1} for CO-Ru^0. But it shows another CO-Ru^0 band at around 2020 cm^{-1}, which was very weak and the absorbance decreased with increasing temperature, indicating the poor thermal stability at higher temperature. When temperature reached 150 °C, the signals of CO-Ru^0 and CO gas bonds seem disappeared, implying that the CO-Ru^0 was transformed to CO-$Ru^{\delta+}$ and/or CO-O_v bonds and the CO adsorption was promoted. For RuO_x-mCeO_2NR-r, there is a stronger CO-Ru^0 at around 2020 cm^{-1}, indicating it has a better CO adsorption ability than RuO_x-CeO_2NR-r at low temperature, which is consistent with H_2-TPR results. With temperature increasing to 150 °C, CO-Ru^0 disappeared and a new band CO-O_v

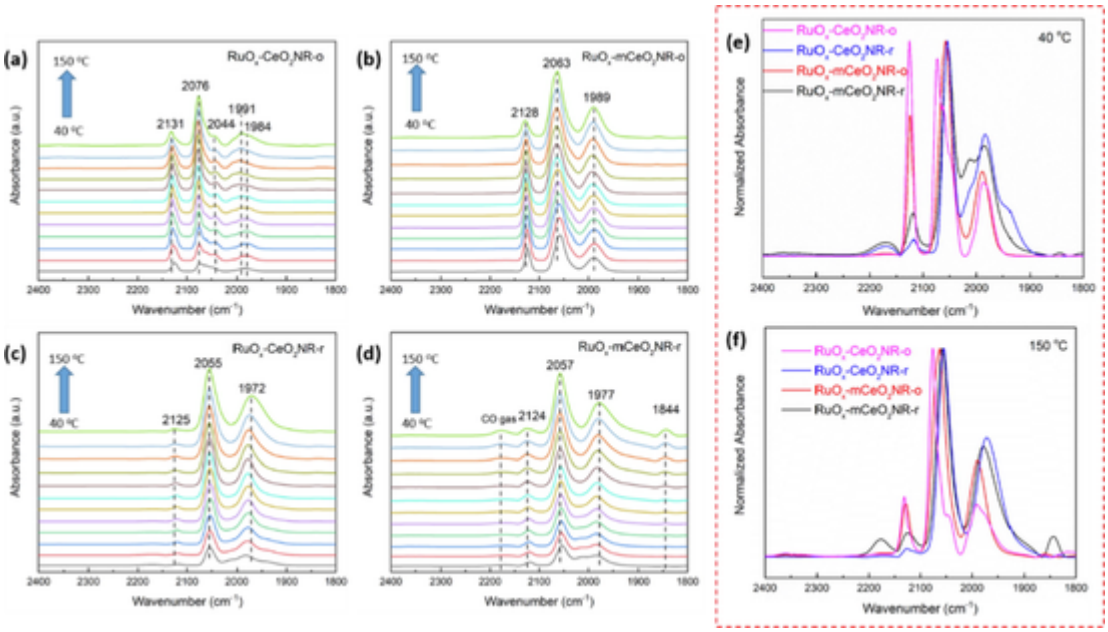

Fig. 5. *In situ* DRIFTS spectra of CO adsorption on (a) RuO_x-CeO_2NR-o, (b) RuO_x-mCeO_2NR-o, (c) RuO_x-CeO_2NR-r and (d) RuO_x-mCeO_2NR-r. The figures of (e) initial and (f) final state for *In-situ* DRIFTS spectra are summarized.

at the Ru-CeO_2 interface formed. Li et al [11] synthesized and ran temperature-dependent *in-situ* DRIFTS of CO oxidation for 5.0 wt% Ru/CeO_2NR. They observed the CO-Ru^0 at 2029 cm^{-1} and also found the increasing absorbance of CO-O_v at 1850 cm^{-1} with decreasing absorbance of CO-Ru^0 when temperature increased, which agrees well with the results in this study. And Kroner et al [45] also demonstrated that bridged CO species were suggested to form with Rh^0 sites, which is similar to the case of Ru/CeO_2 in this study. In addition, the bridged CO shows excellent activity for the oxidation of CO, even better than the linear bonded CO in the case of FeO_x/Pt/TiO_2 catalysts with H_2 flow. Therefore, both the strong CO-Ru^0 bond at low temperature and the bridged CO adsorption CO-O_v at high temperature attribute to the outstanding activity of CO catalytic oxidation.

Similar to the temperature dependent *in-situ* DRIFTS as shown in Fig. 6 **(a ~ d)**, the assignment of time dependent *in-situ* DRIFTS spectra of CO adsorption for as-prepared Ru catalysts can be concluded that: the peaks at around 2120 cm^{-1}/2060 cm^{-1} for CO adsorption spectra is for the multicarbonyl species formed with CO ligands to $Ru^{\delta+}$ sites. The bands at around 2020 cm^{-1} for RuO_x-CeO_2NR-r and RuO_x-mCeO_2NR-r are associated to linearly adsorbed CO with Ru^0. The peaks at 1990 cm^{-1} and 1980 cm^{-1} are associated with the CO adsorbed on oxygen vacancies and bridged CO bonded to Ru at Ru-CeO_2 interface, respectively. The band at 1873 cm^{-1}/1844 cm^{-1} can be assigned to the bridged CO bonded to oxygen vacancy.

By comparison of the time-dependent DRIFTS spectra of CO adsorption on two oxidized Ru catalysts, the $RuO_x$$CeO_2$NR-o shows two CO-$O_v$ peaks at 1873 cm^{-1} and 1844 cm^{-1} different from those of RuO_x-

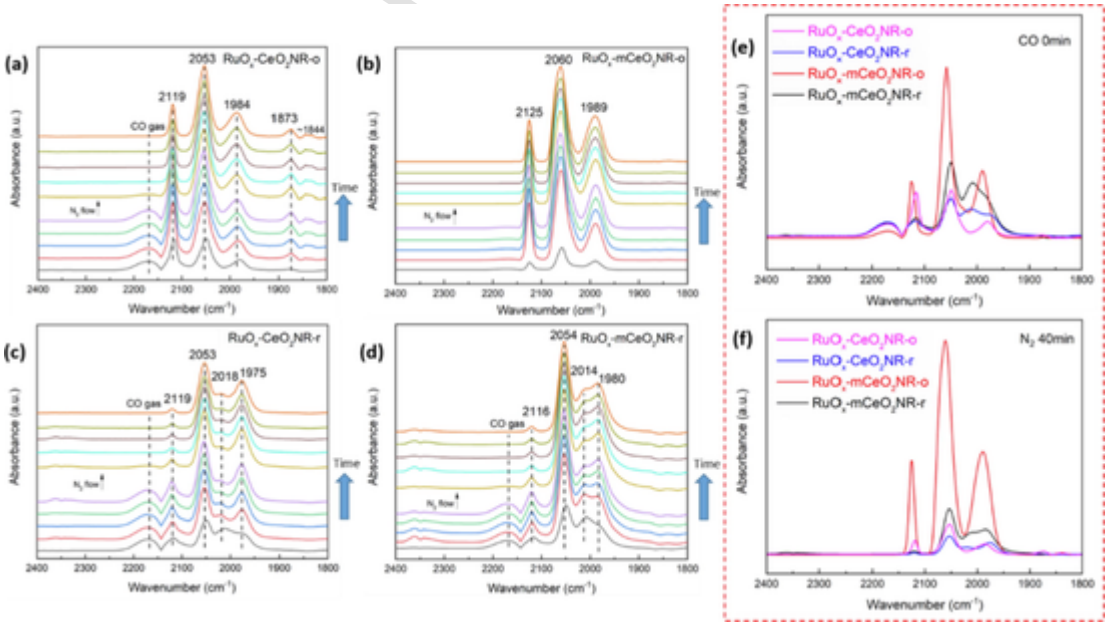

Fig. 6. Time-dependent *in-situ* DRIFTS spectra of CO adsorption on (a) RuO_x-CeO_2NR-o, (b) RuO_x-mCeO_2NR-o, (c) RuO_x-CeO_2NR-r and (d) RuO_x-mCeO_2NR-r. (e) and (f) compare the initial and final state for *in situ* DRIFTS spectra.

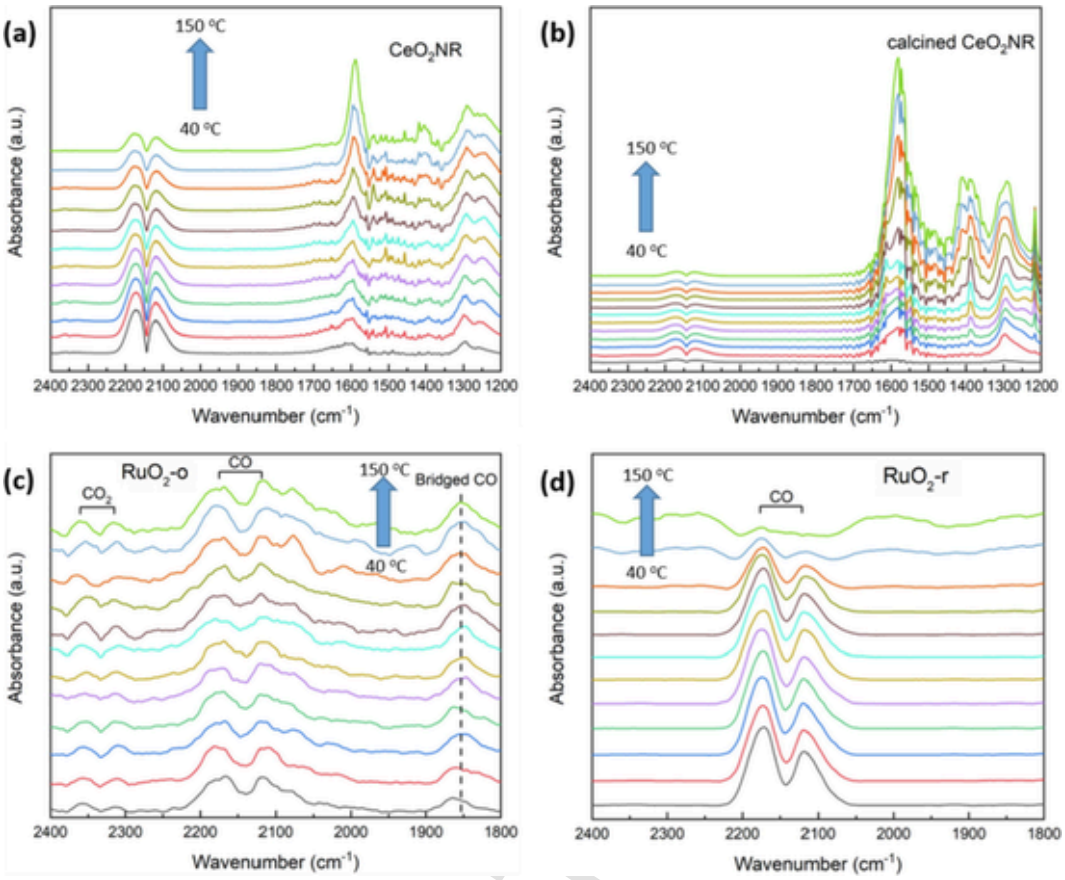

Fig. 7. Temperature-dependent *in situ* DRIFTS spectra of CO adsorption on (a) CeO_2NR, (b) calcined CeO_2NR, (c) commercial RuO_2-o and (d) commercial RuO_2-r.

mCeO_2NR-o. The first profiles (CO for 0 mins) and last profiles (N_2 for 40 mins) of the time-dependent *in-situ* DRIFTS spectra are summarized in Fig. 6 **(e-f)**. The absorbance of RuO_x-mCeO_2NR-o is significantly higher than RuO_x-CeO_2NR-o at the initial state (CO for 0 mins) and this difference is kept to final state (N_2 for 40 mins). This enhanced CO adsorption ability may be owing to the extra CO adsorption to formate species with chemisorbed oxygen induced by the $NaBH_4$ modification. For the reduced Ru catalyst samples, there are two peaks at 2018 cm^{-1} and 2014 cm^{-1}, which correspond to the CO-Ru^0 bonds for RuO_x-CeO_2NR-r and RuO_x-mCeO_2NR-r, respectively. The absorbance of this CO-Ru^0 bond for RuO_x-mCeO_2NR-r is much larger than that for RuO_x-CeO_2NR-r, which is consistent with the DRIFTS spectra of the temperature-dependent results. In addition, this bond existed at the initial state and was not be transferred during the whole process, indicating the strong bonding energy between CO molecules and Ru^0 sites, which can only be destroyed at high temperature. By comparison for the dominated bands at around 2120 cm^{-1}/2060 $cm^{-1}$of the samples before and after reduction, the RuO_x-CeO_2NR-o sample shows higher absorbance than the RuO_x-CeO_2NR-r sample, and the RuO_x-mCeO_2NR-o shows higher absorbance than the RuO_x-mCeO_2NR-r sample, both in the first and the last profiles. The result of this order is similar to the previous results including the H_2 consumption and concentration of Ru^{n+}, indicating that the Ru species shown lower valence state express better reducibility and CO adsorption capability.

However, according to the temperature-dependent *in-situ* DRIFTS spectra of CO adsorption for CeO_2NR, calcined CeO_2NR, commercial RuO_2-o and commercial RuO_2-r in Fig. 7 **(a-d)**, there are no relatively strong CO adsorption bonds can be observed at the region between 2200 cm^{-1} to 1800 cm^{-1} except for the signals of gas-phase CO, when compared with the CeO_2NR supported Ru catalysts. This is consistent with Liu et al's work [7] that there is very weak or no significant CO adsorption behaviour for pristine RuO_2 compared with the supported one. These results indicate that the strong interaction between RuO_x and CeO_2NR helped reinforce the CO adsorption on Ru sites at the RuO_x-CeO_2 interface. These CO species formed with that interaction enhanced the migration of CO during CO oxidation and finally promoted the activity of the Ru catalysts for catalytic reaction.

3.4. CO oxidation performance

Fig. 8 **(a)** shows the CO light-off profiles for four CeO_2NR supported Ru catalysts. It can be noted that the sequence of CO conversion for 100%: RuO_x-mCeO_2NR-o (over 400 °C) > RuO_x-CeO_2NR-o (278 °C) > RuO_x-CeO_2NR-r (273 °C) > RuO_x-mCeO_2NR-r (176 °C), which agrees with the on-set temperature results (Fig. 3**(b)**) from H_2-TPR. Even though RuO_x-mCeO_2NR-o exhibited the highest CO absorbance intensity for time-dependent *in-situ* DRIFTS, the reduced Ru catalysts present relatively higher conversion at low temperature region (below 100 °C) owing to the CO-Ru^0 bonds at around 2020 cm^{-1} for temperature dependent *in-situ* DRIFTS. In addition, the presence of CO-Ru^0 sites at around 2044 cm^{-1} for RuO_x-CeO_2NR-o leads to the high activity at low temperature when compared to RuO_x-mCeO_2NR-o. When temperature is above 100 °C, there is no CO-Ru^0 adsorption pattern for all Ru catalysts. But the particular formation of CO-O_v on Ru-CeO_2 interface for RuO_x-mCeO_2NR-r reinforces the further CO adsorption and finally promotes the CO catalytic oxidation reaction, leading to the lowest conversion temperature for a complete oxidation. The apparent activation energies for CeO_2NR supported Ru catalysts are shown in Fig. 8**(b)**. The values of the activation energies for Ru/CeO_2NR-o, Ru/CeO_2NR-r, Ru/mCeO_2NR-o, and Ru/mCeO_2NR-r are 34.5, 59.4, 43.6, and 31.2 kJ/mol, respectively. This result suggests that these Ru catalysts were activated by the reduction treatment, which is consistent with the *in-situ* DRIFTS results that the presence of new Ru state and extra

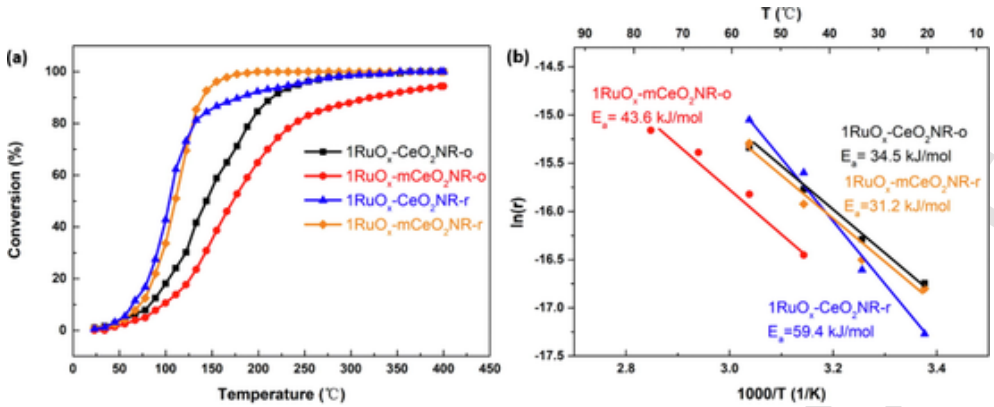

Fig. 8. (a) CO conversion of unmodified/modified CeO_2NR supported Ru catalysts and (b) Arrhenius plots.

CO-Ru^0 adsorption promoted the performance of CO oxidation. It should be noted that these activation energies were calculated at different temperature ranges to better fit into the power law rate equation. Fig. S8 shows the stability test results of RuO_x-CeO_2NR-o, RuO_x-$mCeO_2$NR-o, RuO_x-CeO_2NR-r, and RuO_x-$mCeO_2$NR-r. It can be observed that all four catalysts were relatively stable during the dwell time of 24 h, indicating that the $NaBH_4$ etching treatment is a thermally effective and stable method to enhance the catalytic activity of the prepared catalysts for CO oxidation. Fig. S9 shows the comparison results of CO conversion under dry gas and humid gas (1 vol% H_2O) for RuO_x-$mCeO_2$NR-r, which performed better under dry gas, indicating a negative effect of 1 vol% H_2O on CO oxidation.

4. Conclusions

In conclusion, unmodified and modified CeO_2NR were synthesized and applied as supports to load 1 wt% of RuO_x catalysts for CO oxidation. It was observed that the chemical etching and reduction treatment highly influenced the CO adsorption behavior and CO oxidation activity. The modified CeO_2NR supported reduced Ru catalysts showed the highest concentration of oxygen vacancies, superior low-temperature reducibility, strongest RuO_x-CeO_2 interaction and highest CO oxidation activity (100 % conversion at 176 °C). However, regarding to RuO_x-CeO_2NR-r, the less amount of Ru^{n+} species on surface and lower reducibility resulted in the inferior catalytic activity. There is a dominating factor contributing to these variances: surface chemical environment of catalyst clusters. XPS revealed the promotion effect of surface oxygen vacancies and XRD exhibited the boosted dispersion of RuO_x species after chemical etching treatment and reduction activation, which lead to more active sites on the surface or at interface. As a result of that, the modified CeO_2NR supported reduced Ru catalysts performed better ability to trap and anchor RuO_x species on surface, resulting in stronger interaction between RuO_x and CeO_2 support. *In-situ* DRIFTS presented that oxygen species and Ru^{n+} species on surface with strong interaction remarkably enhanced the CO adsorption capability for CO oxidation, which is crucial for the low temperature CO oxidation reaction with Ru/CeO_2 catalysts.

CRediT authorship contribution statement

Yifan Wang: Investigation, Methodology, Formal analysis, Writing – original draft, Writing – review & editing. **Ruigang Wang:** Conceptualization, Investigation, Methodology, Supervision, Formal analysis, Writing – review & editing, Funding acquisition.

Declaration of Competing Interest

The authors declare that they have no known competing financial interests or personal relationships that could have appeared to influence the work reported in this paper.

Acknowledgment

This work is supported by National Science Foundation (CBET 1856729 and IIP 2044733). The use of TEM facilities at the Alabama Analytical Research Center (AARC) of The University of Alabama is gratefully acknowledged. The authors also gratefully acknowledge the University of Alabama College of Engineering and College of Arts and Sciences' shared analytical facility for providing the use of a Fourier transform infrared spectrometer.

Appendix A. Supplementary material

Supplementary data to this article can be found online at https://doi.org/10.1016/j.jcis.2022.01.062.

References

[1] B.o. Huang, H. Kobayashi, T. Yamamoto, S. Matsumura, Y. Nishida, K. Sato, K. Nagaoka, S. Kawaguchi, Y. Kubota, H. Kitagawa, Solid-Solution Alloying of Immiscible Ru and Cu with Enhanced CO Oxidation Activity, J. Am. Chem. Soc. 139 (13) (2017) 4643–4646.
[2] C. Wang, S. Liu, D. Wang, Q. Chen, Interface engineering of Ru–Co_3O_4 nanocomposites for enhancing CO oxidation, J. Mater. Chem. A 6 (23) (2018) 11037–11043.
[3] Y.H. Kim, E.D. Park, The effect of the crystalline phase of alumina on the selective CO oxidation in a hydrogen-rich stream over Ru/Al2O3, Appl. Catal. B 96 (1–2) (2010) 41–50.
[4] R. Wang, P.A. Crozier, R. Sharma, Structural Transformation in Ceria Nanoparticles during Redox Processes, J. Phys. Chem. C 113 (14) (2009) 5700–5704.
[5] Z. Liu, J. Li, R. Wang, CeO_2 nanorods supported M-Co bimetallic oxides (M = Fe, Ni, Cu) for catalytic CO and C_3H_8 oxidation, J. Colloid Interface Sci. 560 (2020) 91–102.
[6] H. Huang, Q. Dai, X. Wang, Morphology effect of Ru/CeO_2 catalysts for the catalytic combustion of chlorobenzene, Appl. Catal. B 158–159 (2014) 96–105.
[7] Z. Liu, Y. Lu, M.P. Confer, H. Cui, J. Li, Y. Li, Y. Wang, S.C. Street, E.K. Wujcik, R. Wang, Thermally Stable RuO x–CeO_2 Nanofiber Catalysts for Low-Temperature CO Oxidation, ACS Appl. Nano Mater. 3 (8) (2020) 8403–8413.
[8] Y. Ma, P. Ou, Z. Wang, A. Zhu, L. Lu, Y. Zhang, W. Zeng, J. Song, J. Pan, Interface engineering in CeO_2 (111) facets decorated with CdSe quantum dots for photocatalytic hydrogen evolution, J. Colloid Interface Sci. 579 (2020) 707–713.
[9] J. Li, Z. Liu, R. Wang, Support structure and reduction treatment effects on CO oxidation of SiO2 nanospheres and CeO_2 nanorods supported ruthenium catalysts, J. Colloid Interface Sci. 531 (2018) 204–215.
[10] L. Li, L.i. Song, H. Wang, C. Chen, Y. She, Y. Zhan, X. Lin, Q.i. Zheng, Water-gas shift reaction over CuO/CeO_2 catalysts: Effect of CeO_2 supports previously prepared by precipitation with different precipitants, Int. J. Hydrogen Energy 36 (15) (2011) 8839–8849.
[11] J. Li, Z. Liu, D.A. Cullen, W. Hu, J. Huang, L. Yao, Z. Peng, P. Liao, R. Wang, Distribution and Valence State of Ru Species on CeO_2 Supports: Support Shape Effect and Its Influence on CO Oxidation, ACS Catal. 9 (12) (2019) 11088–11103.

[12] Y. She, Q.i. Zheng, L. Li, Y. Zhan, C. Chen, Y. Zheng, X. Lin, Rare earth oxide modified CuO/CeO_2 catalysts for the water–gas shift reaction, Int. J. Hydrogen Energy 34 (21) (2009) 8929–8936.
[13] Y. Tanaka, T. Utaka, R. Kikuchi, T. Takeguchi, K. Sasaki, K. Eguchi, Water gas shift reaction for the reformed fuels over Cu/MnO catalysts prepared via spinel-type oxide, J. Catal. 215 (2) (2003) 271–278.
[14] W. Gao, Z. Zhang, J. Li, Y. Ma, Y. Qu, Surface engineering on CeO_2 nanorods by chemical redox etching and their enhanced catalytic activity for CO oxidation, Nanoscale 7 (27) (2015) 11686–11691.
[15] Z. Han, X. Li, X. Wang, Y.u. Gao, S. Yang, L. Song, J. Dong, X. Pan, Insight into the promoting effect of support pretreatment with sulfate acid on selective catalytic reduction performance of CeO_2/ZrO_2 catalysts, J. Colloid Interface Sci. 608 (2022) 2718–2729.
[16] S. Bae, S. Gim, H. Kim, K. Hanna, Effect of $NaBH_4$ on properties of nanoscale zero-valent iron and its catalytic activity for reduction of p-nitrophenol, Appl. Catal. B 182 (2016) 541–549.
[17] R. Wang, R. Dangerfield, Seed-mediated synthesis of shape-controlled CeO_2 nanocrystals, RSC Adv. 4 (7) (2014) 3615–3620.
[18] S.T. Hossain, Y. Almesned, K. Zhang, E.T. Zell, D.T. Bernard, S. Balaz, R. Wang, Support structure effect on CO oxidation: A comparative study on SiO_2 nanospheres and CeO_2 nanorods supported CuOx catalysts, Appl. Surf. Sci. 428 (2018) 598–608.
[19] Y. Wang, Z. Liu, M.P. Confer, J. Li, R. Wang, In-situ DRIFTS study of chemically etched CeO_2 nanorods supported transition metal oxide catalysts, Molecular Catalysis 509 (2021) 111629, https://doi.org/10.1016/j.mcat.2021.111629.
[20] Y. Wang, Z. Liu, R. Wang, NaBH4 Surface Modification on CeO_2 Nanorods Supported Transition-Metal Catalysts for Low Temperature CO Oxidation, ChemCatChem 12 (17) (2020) 4304–4316.
[21] F. Wang, C. Li, X. Zhang, M. Wei, D.G. Evans, X. Duan, Catalytic behavior of supported Ru nanoparticles on the {1 0 0}, {1 1 0}, and {1 1 1} facet of CeO_2, J. Catal. 329 (2015) 177–186.
[22] J. Jones, H. Xiong, A.T. DeLaRiva, E.J. Peterson, H. Pham, S.R. Challa, G. Qi, S. Oh, M.H. Wiebenga, X.I.P. Hernández, Thermally stable single-atom platinum-on-ceria catalysts via atom trapping, Science 353 (6295) (2016) 150–154.
[23] S. Wu, Y.u. Yang, C. Lu, Y. Ma, S. Yuan, G. Qian, Soot Oxidation over CeO_2 or Ag/CeO_2: Influences of Bulk Oxygen Vacancies and Surface Oxygen Vacancies on Activity and Stability of the Catalyst, Eur. J. Inorg. Chem. 2018 (25) (2018) 2944–2951.
[24] H.Y. Kim, H.M. Lee, G. Henkelman, CO Oxidation Mechanism on CeO_2-Supported Au Nanoparticles, J. Am. Chem. Soc. 134 (3) (2012) 1560–1570.
[25] W. Song, A.S. Poyraz, Y. Meng, Z. Ren, S.-Y. Chen, S.L. Suib, Mesoporous Co_3O_4 with Controlled Porosity: Inverse Micelle Synthesis and High-Performance Catalytic CO Oxidation at −60 °C, Chem. Mater. 26 (15) (2014) 4629–4639.
[26] C.-W. Tang, L.-C. Hsu, S.-W. Yu, C.-B. Wang, S.-H. Chien, In situ FT-IR and TPD-MS study of carbon monoxide oxidation over a CeO_2/Co_3O_4 catalyst, Vib. Spectrosc. 65 (2013) 110–115.
[27] J. Li, G. Lu, G. Wu, D. Mao, Y. Wang, Y. Guo, Promotional role of ceria on cobaltosic oxide catalyst for low-temperature CO oxidation, Catal. Sci. Technol. 2 (9) (2012) 1865–1871.
[28] Y. Yu, Z. Dong, L. Tan, N. He, R. Tang, J. Fang, H. Chen, Enhanced hydrogen evolution reaction in alkaline solution by constructing strong metal-support interaction on Pd-CeO2-x-NC hybrids, J. Colloid Interface Sci. 611 (2022) 554–563.
[29] W.C. Chueh, A.H. McDaniel, M.E. Grass, Y. Hao, N. Jabeen, Z. Liu, S.M. Haile, K.F. McCarty, H. Bluhm, F. El Gabaly, Highly Enhanced Concentration and Stability of Reactive Ce^{3+} on Doped CeO_2 Surface Revealed In Operando, Chem. Mater. 24 (10) (2012) 1876–1882.
[30] K. Kośmider, V. Brázdová, M.V. Ganduglia-Pirovano, R. Pérez, Do Au Atoms Titrate Ce^{3+} Ions at the CeO_2–x(111) Surface? J. Phys. Chem. C 120 (2) (2016) 927–933.
[31] Z. Liu, J. Li, M. Buettner, R.V. Ranganathan, M. Uddi, R. Wang, Metal-Support Interactions in CeO_2- and SiO_2-Supported Cobalt Catalysts: Effect of Support Morphology, Reducibility, and Interfacial Configuration, Acs Appl. Mater. Interfaces 11 (18) (2019) 17035–17049.
[32] Z.-Y. Pu, X.-S. Liu, A.-P. Jia, Y.-L. Xie, J.-Q. Lu, M.-F. Luo, Enhanced Activity for CO Oxidation over Pr- and Cu-Doped CeO_2 Catalysts: Effect of Oxygen Vacancies, J. Phys. Chem. C 112 (38) (2008) 15045–15051.
[33] Y.u. Guo, S. Mei, K. Yuan, D.-J. Wang, H.-C. Liu, C.-H. Yan, Y.-W. Zhang, Low-Temperature CO_2 Methanation over CeO_2-Supported Ru Single Atoms, Nanoclusters, and Nanoparticles Competitively Tuned by Strong Metal-Support Interactions and H-Spillover Effect, ACS Catal. 8 (7) (2018) 6203–6215.
[34] L.j. Atanasoska, W.E. O'grady, R.T. Atanasoski, F.H. Pollak, The surface structure of RuO_2: A leed, auger and XPS study of the (110) and (100) faces, Surf. Sci. 202 (1–2) (1988) 142–166.
[35] S. Bhaskar, P.S. Dobal, S.B. Majumder, R.S. Katiyar, X-ray photoelectron spectroscopy and micro-Raman analysis of conductive RuO_2 thin films, J. Appl. Phys. 89 (5) (2001) 2987–2992.
[36] K. Qadir, S.H. Joo, B.S. Mun, D.R. Butcher, J.R. Renzas, F. Aksoy, Z. Liu, G.A. Somorjai, J.Y. Park, Intrinsic relation between catalytic activity of CO oxidation on Ru nanoparticles and Ru oxides uncovered with ambient pressure XPS, Nano Lett. 12 (11) (2012) 5761–5768.
[37] J. Assmann, V. Narkhede, L. Khodeir, E. Löffler, O. Hinrichsen, A. Birkner, H. Over, M. Muhler, On the nature of the active state of supported ruthenium catalysts used for the oxidation of carbon monoxide: steady-state and transient kinetics combined with in situ infrared spectroscopy, J. Phys. Chem. B 108 (38) (2004) 14634–14642.
[38] G. Yokomizo, C. Louis, A. Bell, An infrared study of CO adsorption on reduced and oxidized $RuSiO_2$, J. Catal. 120 (1) (1989) 1–14.
[39] C.H.F. Peden, D.W. Goodman, M.D. Weisel, F.M. Hoffmann, In-situ FT-IRAS study of the CO oxidation reaction over Ru (001): I. Evidence for an Eley-Rideal mechanism at high pressures? Surf. Sci. 253 (1–3) (1991) 44–58.
[40] S.Y. Chin, C.T. Williams, M.D. Amiridis, FTIR Studies of CO Adsorption on Al_2O_3- and SiO_2-Supported Ru Catalysts, J. Phys. Chem. B 110 (2) (2006) 871–882.
[41] J. Aßmann, E. Löffler, A. Birkner, M. Muhler, Ruthenium as oxidation catalyst: bridging the pressure and material gaps between ideal and real systems in heterogeneous catalysis by applying DRIFT spectroscopy and the TAP reactor, Catal. Today 85 (2–4) (2003) 235–249.
[42] H.-T. Chen, First-principles study of CO adsorption and oxidation on Ru-doped CeO_2 (111) surface, J. Phys. Chem. C 116 (10) (2012) 6239–6246.
[43] G.J. Kim, S.M. Lee, S. Chang Hong, S.S. Kim, Active oxygen species adsorbed on the catalyst surface and its effect on formaldehyde oxidation over Pt/TiO2 catalysts at room temperature; role of the Pt valence state on this reaction? RSC Adv. 8 (7) (2018) 3626–3636.
[44] L.F. Bobadilla, A. Muñoz-Murillo, O.H. Laguna, M.A. Centeno, J.A. Odriozola, Does shaping catalysts modify active phase sites? A comprehensive in situ FTIR spectroscopic study on the performance of a model Ru/Al2O3 catalyst for the CO methanation, Chem. Eng. J. 357 (2019) 248–257.
[45] A.B. Kroner, M.A. Newton, M. Tromp, O.M. Roscioni, A.E. Russell, A.J. Dent, C. Prestipino, J. Evans, Time-resolved, in situ DRIFTS/EDE/MS studies on alumina-supported rhodium catalysts: effects of ceriation and zirconiation on rhodium-CO interactions, Chemphyschem : A Eur. J. Chem. Phys. Phys. Chem. 15 (14) (2014) 3049–3059.